INTERPRETATION OF DARK CURRENT EXPERIMENTAL RESULTS IN HZB SC RF GUN*

V. Volkov, BINP SB RAS, Novosibirsk, Russia

R. Barday, T. Kamps, J. Knobloch, A. Matveenko, A. Neumann, HZB, Berlin, Germany

Abstract

The experimental dark current measurement results are obtained on HZB SC RF gun. The field emitters are considered to be random defects on the back wall of the cavity. Conducting wires with 1 micron length, blobs of 200 micron diameter and "tip on tip" combination of them are taken as dark current emitters in the cavity. RF fields were calculated with CLANS program. The dynamic simulation of dark currents from these emitters fit experimental data. The emitter heating power by RF induced current is four orders of magnitude larger than by the field emitted dark current. The RF induced emitter temperature is proportional to $\omega^{1/2}$ which explains the accelerating gradient limit of a cavity like Kilpatrik law. The RF processing by high order modes seems to be promising.
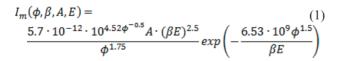
INTRODUCTION

At the end of 2011 experiments with a superconducting *1.3 GHz* RF gun having Pb photocathode were carried out at HZB. The dark current limits the accelerating gradient in the RF gun [1]. Dark current studies were an important part of these experiments.

The electrons starting from emitters on the back wall near the cavity axis and on the cathode can reach the Faraday cup and YAG-screen at 1.56 m from the cathode. Two sets of data are considered: the current vs. the cavity field gradient dependency and the image of the dark current on the YAG-screen.

DARK CURRENT FEATURES

Fowler-Nordheim Data Fitting

Experimental data of the dark current on the accelerating field amplitude were fitted by the Fowler-Nordheim (FN) formula [2]:

$$I_m(\phi, \beta, A, E) = \frac{5.7 \cdot 10^{-12} \cdot 10^{4.52\phi^{-0.5}} A \cdot (\beta E)^{2.5}}{\phi^{1.75}} exp\left(-\frac{6.53 \cdot 10^9 \phi^{1.5}}{\beta E}\right) \quad (1)$$

where ϕ=4.4 eV is the work function of bulk niobium substrate, β is a so called field enhancement factor, A is the emitter tip area, m^2, E is the surface electric RF field, V/m.
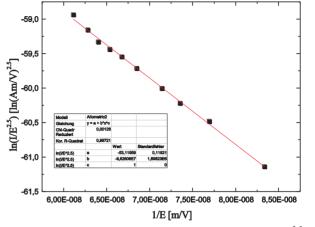
In the Fig. 1 the fitted data is presented.

Figure 1: The dark current data in coordinate's *ln(I/E²·⁵)* vs. *1/E* fitted by FN Eq.1. The FN parameters are: ϕ = 4.4 eV, β = 626, A = 1.43·10⁻²⁰ m²

Fowler-Nordheim dependency of the dark current on the accelerating gradient predicts very high enhancement factor of about *600* and too small emitter tip area of about *10⁻²⁰ m²*. Some assumptions of an emitter nature to explain these facts are required. We consider here the following assumption: an emitter has a complex structure named "tip on tip" [3] consisting of two unequal parts.

Emitter Structure Modelling

The complex structure of emitters consisting on a thin wire connected to a blob is considered. Such emitters named "tip on tip" have a high field enhancement factor. We have numerically simulated following physically possible [4] emitter structures: wire with the length *L=1μm* and radius *r=0.1 μm* ("W10"), wire with *L=1 μm* and *r=0.01 μm* ("W100"), the blob with *100 μm* radius ("Blob"), and the wires connected to the blob ("B&W10", "B&W100"). The first two structures are depicted in Figs. 2a, 2b.
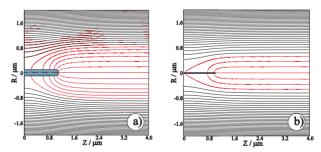

Figure 2: Field lines of the model emitters. a) the wire with *1 μm* length and 0.1 μm radius (W10), b) the wire with *1 μm* length and 0.01 μm radius (W100).

In Table 1 the calculated enhancement factors of these emitters are presented. As one would expect, a wire enhancement factor is about of $\beta \approx L/r$, and the enhancement factor of complex emitters is the product of their intrinsic enhancement factors: $\beta \rightarrow \beta_{Blob} \times \beta$.

Thermal Effects Analysis

Test parameters of emitters (β and A) were changing during the experiments. They had become $\beta \approx 200$ and $A \approx 6.7 \cdot 10^{-16} \, m^2$ by the end of the experiments. This is probably due to the RF and laser processing [1]. The main part of the RF processing mechanism is the emitter heating [3]. We consider two reasons of the emitter heating: the heating by the RF induced current and the heating by the FN dark current.

The example of the RF induced current heating is the electric circuit of a resistor with a capacity series-connected to an RF current source. The capacity electric RF field is equivalent to the part of cavity RF electric field that is close to the emitter surface (see Figs. 2a, 2b-red color). According to Ampere`s law ($H \approx 0$) the RF induced current in the emitter is:

$$I = \left| \int_s \frac{\partial \overline{D_s}}{\partial t} \cdot d\overline{S} \right| = \omega \varepsilon_o \int_s \overline{E_s} \cdot d\overline{S} \approx \omega \varepsilon_o E \pi L^2 \qquad (2)$$

where the integration is made over the emitter surface S. $D_s = \varepsilon_o E_s \cdot e^{j\omega t}$ is the emitter surface electric field. The integral value is approximately the product of the external electric field E and the area of the circle with radius L (L is the emitter length). This is demonstrated in Figs. 2a, 2b where the (red) electric force lines terminated on emitters come from the region of the circle with radius L.

Since the skin effect in a normal conducting metal is more than 2 μm at 1.3 GHz, the RF field penetrates into emitters (see Figs. 3a, 3b). Therefore, the emitter resistance is given by $R \approx \rho L/\pi r^2$ and the dissipated power is $P_{RF} \approx RI^2/2$. After insertion and assuming $L/r \approx \beta$ we have

$$P_{RF} \approx \frac{\pi}{2} \rho (\varepsilon_o E)^2 \omega^2 \beta^5 r^3, \qquad (3)$$

where ρ is emitter resistance in *Ohm·m*.

For the complex emitter we must replace in Eq.3 $E \rightarrow \beta_{Blob} E$ and $\beta \rightarrow \beta/\beta_{Blob}$. The power dissipated in the complex emitter is

$$P_{B\&W} = P_{RF} / \beta_{Blob}^3 \qquad (4)$$

CLANS [5] simulated RF power dissipation taking into account the skin effect, is presented in Table 1. The power dissipated due to the DC dark current (I_{FN}) and some of its harmonics of the main frequency on the emitter resistance is approximately

$$P_{FN} \approx 10 \cdot I_{FN}^2 \rho \frac{L}{\pi r^2} \approx 10 \cdot I_{FN}^2 \rho \frac{\beta}{\pi r}, \qquad (5)$$

where numerical coefficient 10 is directly compatible for dark current pulse of 10º RMS width. This power with the average dark current of about *0.1 μA* is 4 orders of magnitude lower than P_{RF} (see Table 1).

Table 1: CLANS calculated characteristics of copper ($\rho = 1.694 \cdot 10^{-8} \, Ohm \cdot m$) emitters at $E = 20 \, MV/m$

Emitter	W10	W100	B&W10	B&W100
β	12.7	77	53	326
E_{peak}, MV/m	238.6	1453	1005	6138
P_{RF}, W	$1.7 \cdot 10^{-12}$	$2.2 \cdot 10^{-11}$	$3.4 \cdot 10^{-11}$	$4.3 \cdot 10^{-10}$
$P_{FN \, of \, 0.1 \, μA}$, W	$4.6 \cdot 10^{-16}$	$5.4 \cdot 10^{-14}$	$4.6 \cdot 10^{-16}$	$5.4 \cdot 10^{-14}$
T, K	83	158	280	587

The laser processing can be considered as RF processing with a higher frequency. The experiments were made with the laser wave length of $\lambda = 248 \, nm$ ($1.2 \cdot 10^{15} \, Hz$), the intensity of *0.23 mJ/mm^2 (E=62 V/m)*, and pulse width of *5 ns* [1]. This pulse width (τ) is sufficient to heat a Pb emitter (with density of $\delta = 11 \cdot 10^3 \, kg/m^3$, specific heat capacity of $c_v = 130 \, J/kgK$, and $\beta = 600$) up to temperature $T = 1000K$ and melt it.

$$\tau \approx \frac{2\delta c_v T}{\rho \beta^4 (\varepsilon_o \omega E)^2} \qquad (6)$$

Emitter Temperature

We consider the thermal conductivity along the emitter to the surface is negligible. The dissipated power (P) in the emitter radiates through its surface $S = 2\pi r L \approx 2\pi r^2 \beta$. The emitter temperature (T) is defined with Stephan-Boltzmann constant (σ) as $P = \sigma T^4 S = \sigma T^4 2\pi r^2 \beta$.

Using Eq.3 for the P we get the wire emitter temperature due to RF field as

$$T_{RF} = \beta \cdot [(\varepsilon_o E)^2 \omega^2 \rho r / 4\sigma]^{1/4} \qquad (7)$$

The temperature of a copper wire emitter with the experimentally found $\beta = 626$ is $T = 1290K$. For a complex emitter this temperature will be less factor $\beta_{Blob}^{3/4}$ according to Eq.4, i.e. $T = 425K$.

According to Eq.7 the emitter temperature grows as $\omega^{1/2}$. We can suppose that the RF processing at HOM frequency is more effective one. According to Kilpatrick law the accelerating gradient limit of a cavity is proportional to $\sim \omega^{1/2}$. Probably, the obtained field limit at HOM RF processing keeps the same value at the (lower) fundamental frequency. Certainly the places of peak surface electric field must be the same for both the operating mode and the HOM.

Using Eq.5 for the P_{FN} we get the wire emitter temperature due to FN current as

$$T_{FN} = \frac{1}{r} \left(I_{FN}^2 \frac{10\rho r}{2\pi \sigma} \right)^{1/4} \qquad (8)$$

The temperature of a copper wire emitter with $I_{FN} = 0.1 \, μA$ and the $r = 10^{-10} \, m$ calculated from the experimental data with the work function of 4.4 eV is $T = 8400K!$ Emitters of such small radius physically cannot exist.

Flying Emitters

Two types of flying emitters were modeled by CLANS (see Figs. 3a, 3b). One of the ends of the emitter attracts by the electric field with the force $F=4\pi\varepsilon_o r^2\beta E^2$. Two of these forces acts in opposite directions and align the emitter along the electric force line. The net force has a nonzero value if the field is nonuniform, i.e. $dE/dL\neq0$. The net force is

$$F = 8\pi\varepsilon_o r^3\beta^2 E\frac{dE}{dL} \qquad (9)$$

Where $\beta\approx L/2r$ is the field enhancement factor of the flying emitter that is factor two lower than in the case when it is connected to a surface.

The flight is possible if this force is larger than the emitter weight, i.e. the flight condition is:

$$\frac{Force}{Weight} = \frac{8\beta\varepsilon_o}{\delta g}E\frac{dE}{ds} \geq 1 \qquad (10)$$

where δ is the emitter mass density, $g=9.8\ m/sec^2$. There are regions in the cavity where this factor goes up to *500*. Maximal attracting force acts close to a blob. For the considered blob and wire emitters this force is 7 orders of magnitude higher than the emitter weight. But the stretching force acting on the flying emitter is too low to destroy the emitter.

So we can consider an emitter as a wire attracted to a blob. This emitter can migrate between blobs. Such emitters can create a long chain.
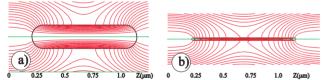

Figure 3: Field distribution near the flying emitters with a) *L/r=10*, b) *L/r=100*. Edited output of the CLANS [5].

DARK CURRENT IMAGE

The image of the dark current on the YAG screen is presented in Fig. 4. The image has a form of a line with one point 'at focus' and cone tails. The RMS tail cone angle is approximately *12°*.

If we consider a small emitter off-axis of the cavity back wall, which emits electrons without angular spread, the screen image would be a thin line. Each point of the line corresponds to a definite launch phase.

The specific form of the dark current image shows that in reality the emitter is a micro-wire connected to a blob having a high field enhancement factor β. The diverging force lines of the electric field originate on the emitter tip. It leads to a cone shaped beam close to the emitter. The screen image of such a beam is a line with one focused point, corresponding to some launch phase, and cone tails. The tail cone angle is relatively big, that can be only due to the complex emitter structure.
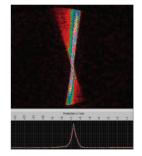

Figure 4: The dark current image on the YAG-screen.

The scheme of the image formation is demonstrated in Fig. 5. It is confirmed by numerical simulations with ASTRA. In this simulation the image charge of emitted electrons in the spherical surface of the emitter tip with the curvature radius r is taken into account. The density of the emitted current has Gaussian radial distribution according to FN dependence on the surface electric field distribution. Results of ASTRA simulation are presented in Table 2. The complex emitter only (B&W) can produce the impact image with the cone angle more than 12° that is found in the experiment and the tip emitting spot radius is of the order of the emitter radius.
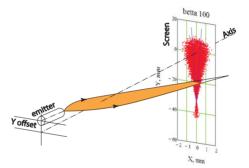

Figure 5: The scheme of some cavity dark current trajectories impacting to the screen. The screen image is obtained by the ASTRA simulation with $Y_{offset}=3\ mm$.

Table 2: RMS cone angles of dark current impact images. RMS tip emitting spot radius is ϱ

ϱ/r	W10	W100	B&W10
0.134	1.82°	1.64°	5.12°
0.268	3.51°	3.2°	10.1°
0.366	4.77°	4.36°	14.2°

REFERENCES

[1] A. Neumann et al. IPAC 2011, San Sebastian, Spain, 2011.

[2] R.H. Fowler, L. Nordheim, Proc. R. Soc. London A 119 (1928), p. 173.

[3] J. Knobloch, Ph.D. Cornell University 1997.

[4] A. Hassanein et al. PRST AB **9**, 062001 (2006).

[5] D.G. Myakishev, V.P. Yakovlev // PAC 1999, New York. – 1999. -- pp. 2775-2777.